



# Numerical Modeling of Precast Concrete Interior Beam-Column Joints with Hybrid Connection System: Model Verification and Parametric Study

Angeline Gunawan<sup>1</sup>, Hartanto Wibowo<sup>2</sup>, and Jimmy Chandra<sup>1</sup> (✉)

<sup>1</sup> Petra Christian University, Jl. Siwalankerto 121-131, Surabaya, Indonesia  
chandra.jimmy@petra.ac.id

<sup>2</sup> Iowa State University, 813 Bissell Road, Ames, IA, USA

**Abstract.** In this study, a finite element model of precast concrete interior beam-column joints with hybrid connection system comprising unbonded post-tensioned strands and bolted steel angles was analyzed. The connection system is expected to exhibit self-centering characteristics, thus minimizing residual drift and providing adequate energy dissipation during seismic events. Furthermore, this study also aims to investigate several parameters affecting the behavior of the hybrid connection system. To achieve this purpose, nonlinear analyses were conducted using two-dimensional finite element model developed in OpenSees. The model was validated with past experimental studies conducted for the hybrid connection system. Subsequently, a parametric study was conducted involving eight key parameters: concrete compressive strength, concrete beam's width, steel angle dimension, steel angle thickness, effective prestressing force ratio, column axial load ratio, and the distance of the first bolt at the column and beam leg from the joint. The analysis results show that the finite element model could simulate quite well the seismic behavior of the hybrid connection system, including the desired self-centering characteristic and sufficient energy dissipation. Moreover, the parametric study shows that the steel angle thickness emerges as the most influential parameter, profoundly impacting moment and energy dissipation capacities.

**Keywords:** Numerical Model · Precast Concrete Interior Beam-Column Joints · Hybrid Connection System · Unbonded Post-Tensioned Strands · Bolted Steel Angles

## 1 Introduction

Building construction has grown to be more resilient and sustainable for a few decades when dealing with post-earthquake rehabilitation. To reduce economic losses and downtime in post-earthquake building reparation, it is indispensable to maintain the damage level to be minimal and to satisfy the enhanced objective requirement criteria according to ASCE 41-13 [1]. Similarly, in FEMA P-58-1 [2], the structural damage is correlated

to residual drift, which also corresponds to the structure reparability. One of the structural systems that has been proven experimentally to achieve minimal residual drift and adequate energy dissipation is the hybrid connection system. This type of system is a combination of unbonded post-tensioned strands and energy dissipation devices.

Prior investigation of the hybrid connection system started with the use of unbonded post-tensioned steel in a precast structure, which was done numerically by Priestley and Tao [3] and experimentally by MacRae and Priestley [4, 5], which allowed self-centering or rocking motion in a controlled manner at the beam and column interface that replaced the plastic hinges mechanism. However, the re-centering system using only post-tensioned steel without energy dissipation devices resulted in bilinear elastic hysteresis with low energy dissipation capacity. Stanton et al. [6] then improved the connection system by combining unbonded post-tensioned steel with external energy dissipation devices. The system is a hybrid connection system, which provides negligible residual displacement and adequate energy dissipation. Further development of hybrid connection systems varies with the type of energy dissipation devices such as lead damper [7], shear bracket [8], corbel connection [9], shape memory alloys [10, 11], buckling restrained reinforcement [12], and friction devices [13]. Although the mentioned energy dissipation devices provide sufficient energy dissipation, complex and advanced devices are likely to be impractical and uneconomical. The bolted steel angle was proven to contribute as a simple and efficient energy dissipation device in moment-resisting frames through experiment studies [14–17]. The bolted steel angle could also act as shear resistance at the contact surface of precast beams and columns and as a concrete beam-crushing protector.

Computational processes, which now are faster and more accessible to simulate structural behavior, are beneficial and efficient compared to experimental methods. Several numerical models for unbonded post-tensioned precast concrete structures with hybrid connection systems have already been proposed [16, 18–22]. However, a detailed numerical model for bolted steel angles as energy dissipation devices in precast moment-resisting frames is limited. The main objective of this study is to develop a numerical model for precast concrete interior beam-column joints with unbonded post-tensioned strands and bolted steel angles. In addition, this study also aims to present a comprehensive parametric study on the performance of the hybrid connection system and factors affecting it. The numerical analysis is conducted using a two-dimensional finite element model in OpenSees software. The varied parameters are concrete compressive strength, concrete beam's width, steel angle dimension, steel angle thickness, effective prestressing force ratio, column axial load ratio, and the distance of the first bolt at the column and beam leg from the joint. It is highly expected that the model developed in this study can simulate well the behavior of the hybrid connection system. Moreover, the results of the parametric study will be used as a basis for designing further experimental studies of the hybrid connection system.

## 2 Numerical Modeling and Model Verification

This section explains the constitutive model of the bolted steel angle and the hybrid connection system in the precast joint model. The steel angle model was verified with the experimental study by Garlock et al. [19]. Then, the verified steel angle model was

applied to the hybrid connection system in the precast joint model. Subsequently, the precast joint model was verified with the experimental study by Cai et al. [22].

## 2.1 Bolted Steel Angle

**Constitutive Model.** In this study, the bolted steel angle was modeled with a truss element. Uniaxial Pinching4 material available in OpenSees was assigned to the truss element. The defined material represents the stress-strain response of the steel angle under cyclic loading. The experimental study by Garlock et al. [19] showed that the bolted steel angle's response under tension and compression loading differed in characteristics. Bilinear behavior develops under tension loading while linear behavior develops under compression loading. Formulas developed by Cai et al. [22] were used to calculate the steel angle's capacity and stiffness under tension and compression loading.

As mentioned, the behavior under tension loading becomes bilinear after the steel angle is yielded. The yield strain is obtained by dividing the yield stress by the elastic modulus of the steel angle. In the inelastic stage, the stiffness of the steel angle was assumed to be 1.25% of the initial elastic modulus. In compression loading, the stiffness of the steel angle ( $K_c$ ) was calculated with Eq. 1, where:  $E_a$  = elastic modulus of the steel angle;  $A_a$  = cross-section area of the steel angle;  $l_{gv}$  = column bolt gage length. Furthermore, the area of the truss element ( $A_e$ ) was calculated using Eq. 2, where:  $t_a$  = thickness of the steel angle;  $b_a$  = total width of the steel angle.

$$K_c = \frac{1}{40} \frac{E_a A_a}{l_{gv}} \quad (1)$$

$$A_e = (1.35 - 0.027t_a) \frac{b_a t_a^2}{2l_{gv}} \quad (2)$$

**Model Verification.** The bolted steel angle model was validated with the experiment conducted by Garlock et al. [19]. In the experiment, there were two specimens tested, L8-58-4 and L6-516-9. The experimental setup and numerical model are shown in Fig. 1 while the specimens' details and material properties are listed in Table 1. The comparison of hysteresis curves between experiment and numerical analyses is shown in Fig. 2. The peak forces of the specimens were predicted well while the initial stiffness of the bolted steel angle in tension loading tends to be underestimated for both specimens. Similarly, the unloading stiffness also tends to be lower as compared to the experimental results. Consequently, the energy dissipation capacity of the model is smaller than the actual specimens. However, overall, the bolted steel angle model is still in good agreement with the experiment results and thus the model can be used in the hybrid connection system. The summary of the bolted steel angle model validation can be seen in Table 2.

## 2.2 Hybrid Connection System

**Numerical Model.** In this study, the finite element model of a precast concrete interior beam-column joint with hybrid connection system is shown in Fig. 3. The model is almost similar to the one used by Cai et al. [16] for exterior beam-column joint. However, there

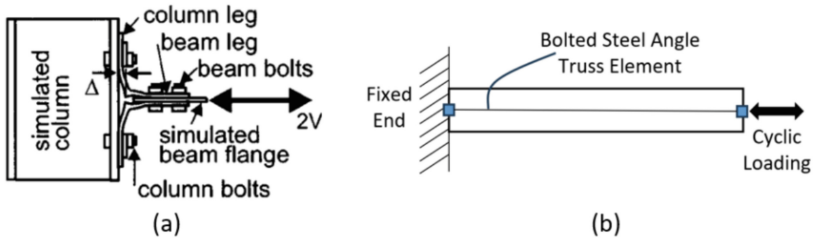


**Fig. 1.** (a) Experimental setup [19]; (b) Numerical model of the bolted steel angle

**Table 1.** Specimens' details and material properties

Specimen	Angle Size	$t_a$	$f_y$
	(mm)	(mm)	(MPa)
L8-58-4	L203 × 203	15.9	332
L6-516-9	L152 × 152	7.9	

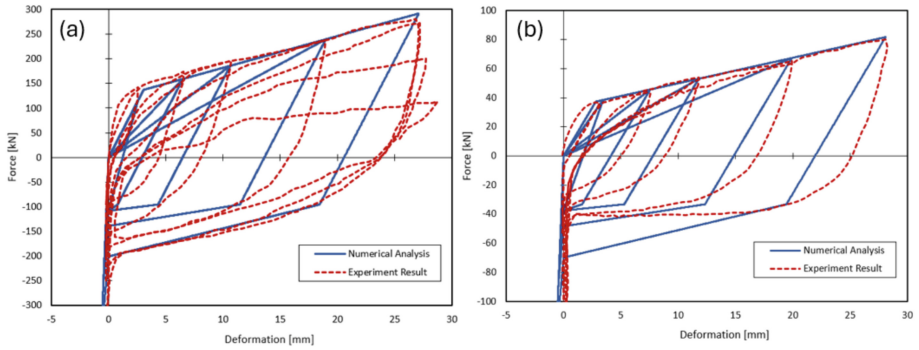


**Fig. 2.** Hysteresis curves comparison; (a) L8-58-4 and (b) L6-516-9

**Table 2.** Summary of the bolted steel angle model validation

Specimen	$P_{max}$ Exp	$P_{max}$ Num	$P_{max}$	ED Exp	ED Num	ED
	(kN)	(kN)	Num/Exp	(kN.m)	(kN.m)	Num/Exp
L8-58-4	280.54	291.97	1.04	7.51	6.32	0.84
L6-516-9	80.20	81.67	1.02	2.12	2.07	0.97

were some modifications introduced to the model used in this study. The beams and columns were modeled using Displacement-Based Beam-Column element available in OpenSees, which considers the distributed plasticity along the element. Fiber section was

used to model the plastic hinge of the element. Concrete02 uniaxial material was chosen to represent concrete material behavior while Steel02 uniaxial material was chosen to represent the longitudinal reinforcement. The transverse confining reinforcement was accounted into confined concrete material of the core fiber while the material properties of cover concrete were equal to those of unconfined concrete material.

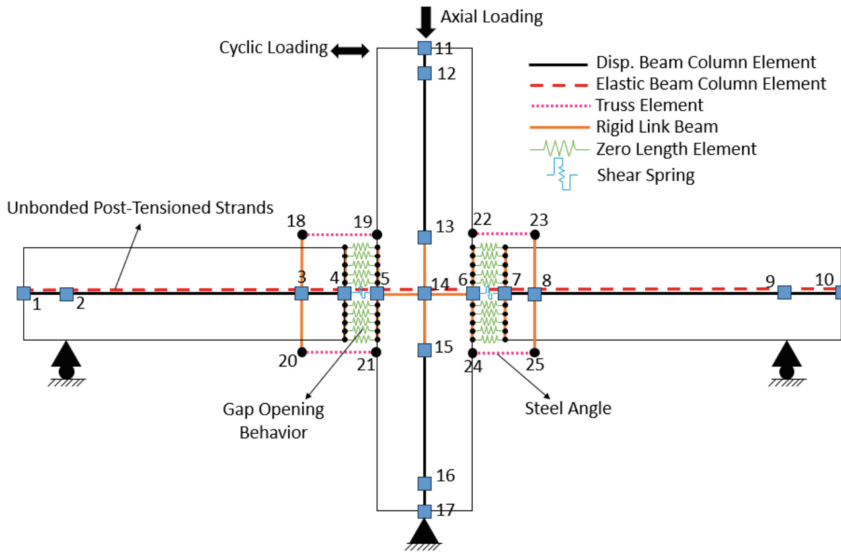


**Fig. 3.** Typical numerical model of the hybrid connection system used in this study

The interior beam-column joint is not expected to experience significant deformation, and therefore the panel zone was modeled as rigid in this study, as opposed to the model by Cai et al. [16] which considers panel zone deformation for exterior beam-column joint. The central node of the panel zone is connected with rigid links to the nodes at the end of beams and columns. As the precast concrete beam-column joint starts to deform due to cyclic loading, at the interface between beams and columns, gap-opening behavior is modeled with multiple zero-length elements. These elements were assigned with Concrete01 material, which had a “compression-only” stress-strain relationship while the tensile strength and stiffness were zero. The unbonded post-tensioned strand was modeled with elastic beam-column element and the area was defined with the total cross-section area of the strands. The post-tensioned force was applied as compression force to the element.

The bolted steel angles at the top and bottom of the beams were modeled as truss elements. As shown in Fig. 3, nodes 18, 20, 23, and 25 are the center of the bolt holes at the precast beams. The bolt holes in the precast columns are represented by nodes 19, 21, 22, and 24. The truss elements which represent the bolted steel angles were assigned to connect these nodes. The constitutive model used for the truss elements has already been explained in the previous section.

**Model Verification.** The unbonded post-tensioned precast joint with bolted steel angles model was validated against the experiment conducted by Cai et al. [22]. The specimen tested is described as follows: the column and beam cross-sectional dimensions are  $400 \times 400$  mm and  $250 \times 450$  mm with 1800 mm length each. The strands are unbonded at the centroid of the beam with total area of  $560 \text{ mm}^2$  and the post-tensioned force is approximately equal to 520 kN. The experimental setup and the numerical model are shown in Fig. 4. Since the experimental setup [22] was to simulate an exterior beam-column joint, zero length elements to simulate gap opening behavior and truss elements to represent the steel angles were put only in the tested beam. There are three specimens that were used to validate the numerical model, and their properties are listed in Table 3. The analysis results show that the numerical model is in good agreement with the experiment data in predicting the yield and ultimate forces. However, the initial and unloading stiffness tend to be overestimated. The comparison of hysteresis curves between numerical analysis and experiment result can be seen in Fig. 5 while the comparison of maximum forces and energy dissipation is listed in Table 4. It can be concluded that the finite element model used can simulate quite well the seismic behavior of the hybrid connection system including self-centering characteristic with sufficient energy dissipation.

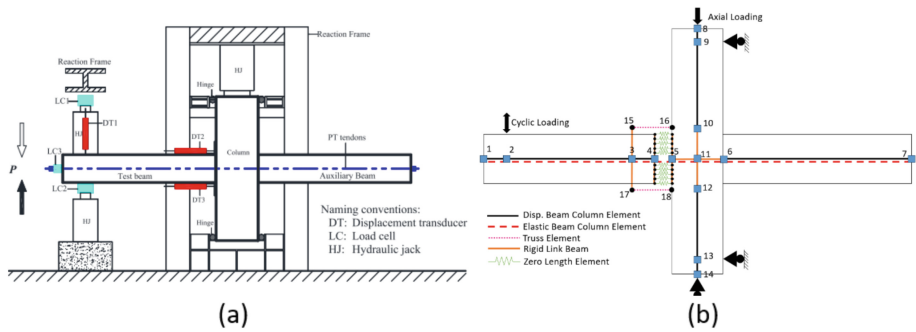


**Fig. 4.** (a) Experimental setup [22]; (b) Numerical model of the hybrid connection system

**Table 3.** Steel angle details and material properties

Specimen	Angle Size	$t_a$	$l_{gv}$	$f_y$
	(mm)	(mm)	(mm)	(MPa)
B450-S520-A1	L180 × 180	12	120	270
B450-S520-A2	L180 × 180	12	140	270
B450-S520-A3	L180 × 110	10	120	281

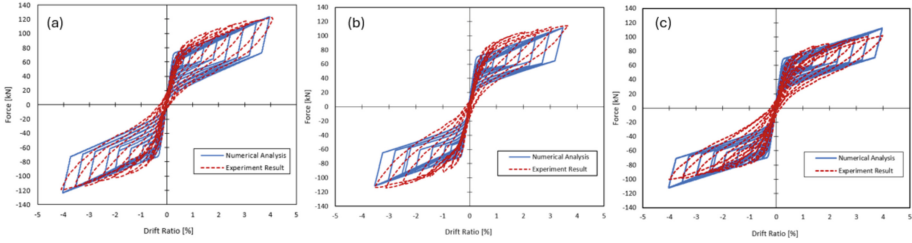


**Fig. 5.** Hysteresis curves comparison of specimen (a) B450-S520-A1, (b) B450-S520-A2, and (c) B450-S520-A3

**Table 4.** Hybrid connection model verification results

Specimen	$P_{max}$ Exp		$P_{max}$ Num		$P_{max}$ Num/Exp		ED Exp	ED Num	ED Num/Exp
	(+)	(-)	(+)	(-)	(+)	(-)			
	(kN)		(kN)				(kN.m)	(kN.m)	
B450-S520-A1	122.1	118.9	123.5	123.6	1.01	1.04	5.89	6.09	1.03
B450-S520-A2	114.3	114.0	111.4	111.4	0.97	0.98	4.15	4.23	1.02
B450-S520-A3	101.8	98.4	112.2	112.2	1.10	1.14	3.80	4.45	1.17

### 3 Parametric Study

The selected parameters in this study are concrete compressive strength ( $f'_c$ ), concrete beam’s width ( $b_b$ ), steel angle dimension ( $L$ ), steel angle thickness ( $t_a$ ), effective post-tensioned force ratio ( $P_{ps}/(f'_c A_{gb})$ ), column axial load ratio ( $P/(f'_c A_{gc})$ ), and the distance of the first bolt at the column ( $l_{gv}$ ) and beam leg ( $El$ ) from the joint. The control specimen is described as follows. The beam and column dimensions are  $400 \times 400$  mm with 1800 mm length for each beam and 2860 mm length for column. The concrete compressive strength is set to be 30 MPa. The applied axial load is equal to  $0.15f'_c A_{gc}$  and the effective post-tensioned force is equal to  $0.09f'_c A_{gb}$ . The steel angle dimension is  $120 \times 120 \times 10$  mm ( $f_y = 270$  MPa) and bolted with 25 mm prestress bar ( $f_u = 880$  MPa). The four strands of  $0.6'' - 7$  wire strands, with the total area of post-tensioned strands being  $560 \text{ mm}^2$ , are located at the centroid of the beam. The specimen details and parameter notations are shown in Fig. 6. For the parametric study, there are two different values for each parameter varied from the control specimen. These values are listed in Table 5.

**Analysis Results.** The results of the parametric study are analyzed throughout each hysteresis curve, initial stiffness and stiffness degradation, energy dissipation capacity, and backbone curve. The analysis results are discussed below.

**Hysteresis Curves.** The hysteresis curves for each specimen are shown in Fig. 7. The results show that parameters influencing the structural behavior of the hybrid connection system are concrete compressive strength, concrete beam’s width, distance of the

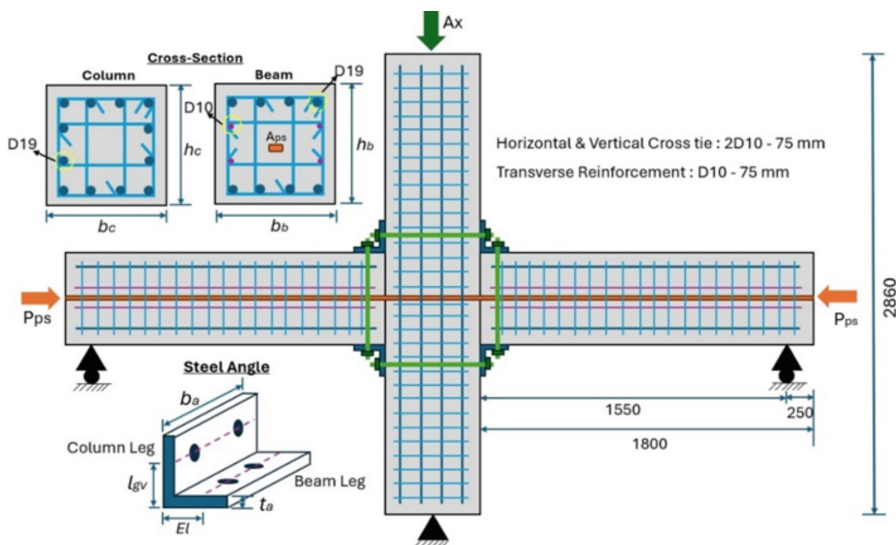


Fig. 6. Cross-section and specimen details for parametric study

first bolt at the column leg, thickness of the bolted steel angle, and the effective post-tensioned force ratio. Higher concrete compressive strength results in higher horizontal force capacity of the connection. This is mainly due to the change in effective post-tensioned force value. In order to keep the effective post-tensioned force same for all specimens ( $0.09f'_c A_{gb}$ ), the specimen with higher concrete compressive strength has higher post-tensioned force value. As a result, this increases the lateral force capacity of the connection. Similarly, concrete beam's width also affects the moment capacity of the connection. A wider beam has more post-tensioned force value as well as wider steel angle ( $b_a$ ). Therefore, a wider beam has higher capacity. The distance of the bolt at the column leg to the joint also affects the lateral force capacity of the connection. As the distance of the bolt increases, the overall steel angle stiffness decreases. Thus, the moment capacity of the hybrid connection system also decreases. In addition, the steel angle thickness also has a significant role in determining the capacity of the connection. As the thickness of the steel angle is larger, the peak horizontal force increases. Lastly, the effective post-tensioned force ratio also affects the capacity of the hybrid connection system. The specimen with higher ratio has higher capacity.

*Initial Stiffness and Stiffness Degradation.* Figure 8 compares the initial stiffness and stiffness degradation of all the models analyzed. The stiffness degradation was evaluated using the secant stiffness for each drift ratio. Specimen ta14 and bb300 are specimens with the highest and lowest stiffness characteristics, respectively. This means that steel angle thickness and concrete beam's width are two main factors that affect the stiffness of the hybrid connection system.

*Energy Dissipation Capacity.* The comparison of energy dissipation capacity between all models analyzed is shown in Fig. 9. It can be seen that the energy dissipation capacity is highly affected by the steel angle thickness and the distance of the first bolt at the column

**Table 5.** Varied parameters in this study

Specimen	Parameters							
	$f'_c$ (MPa)	$l_{gv}$ (mm)	$P/(f'_c A_{gc})$	$L$ (mm)	$t_a$ (mm)	$P_{ps}/(f'_c A_{gb})$	$b_b$ (mm)	$El$ (mm)
Control	30	80	0.15	120 × 120	10	0.09	400	80
fc35	35	80	0.15	120 × 120	10	0.09	400	80
fc25	25	80	0.15	120 × 120	10	0.09	400	80
bb350	30	80	0.15	120 × 120	10	0.09	350	80
bb300	30	80	0.15	120 × 120	10	0.09	300	80
lgv100	30	100	0.15	120 × 120	10	0.09	400	80
lgv60	30	60	0.15	120 × 120	10	0.09	400	80
El100	30	80	0.15	120 × 120	10	0.09	400	100
El60	30	80	0.15	120 × 120	10	0.09	400	60
Dim140	30	80	0.15	140 × 140	10	0.09	400	80
Dim130	30	80	0.15	130 × 130	10	0.09	400	80
ta14	30	80	0.15	120 × 120	14	0.09	400	80
ta12	30	80	0.15	120 × 120	12	0.09	400	80
Pps8	30	80	0.15	120 × 120	10	0.08	400	80
Pps7	30	80	0.15	120 × 120	10	0.07	400	80
Ax20	30	80	0.20	120 × 120	10	0.09	400	80
Ax10	30	80	0.10	120 × 120	10	0.09	400	80

leg, while the other parameters do not affect much. Specimen ta14 has the highest energy dissipation capacity whereas specimen lgv100 has the lowest value.

**Backbone Curves.** The backbone curve results are compared in Fig. 10. The highest peak force at 4.00% drift is achieved by the specimen ta14. On the contrary, the specimen bb300 has the lowest peak force. Indeed, this comparison implies that steel angle

thickness is the most influential parameter for the behavior of the hybrid connection system.

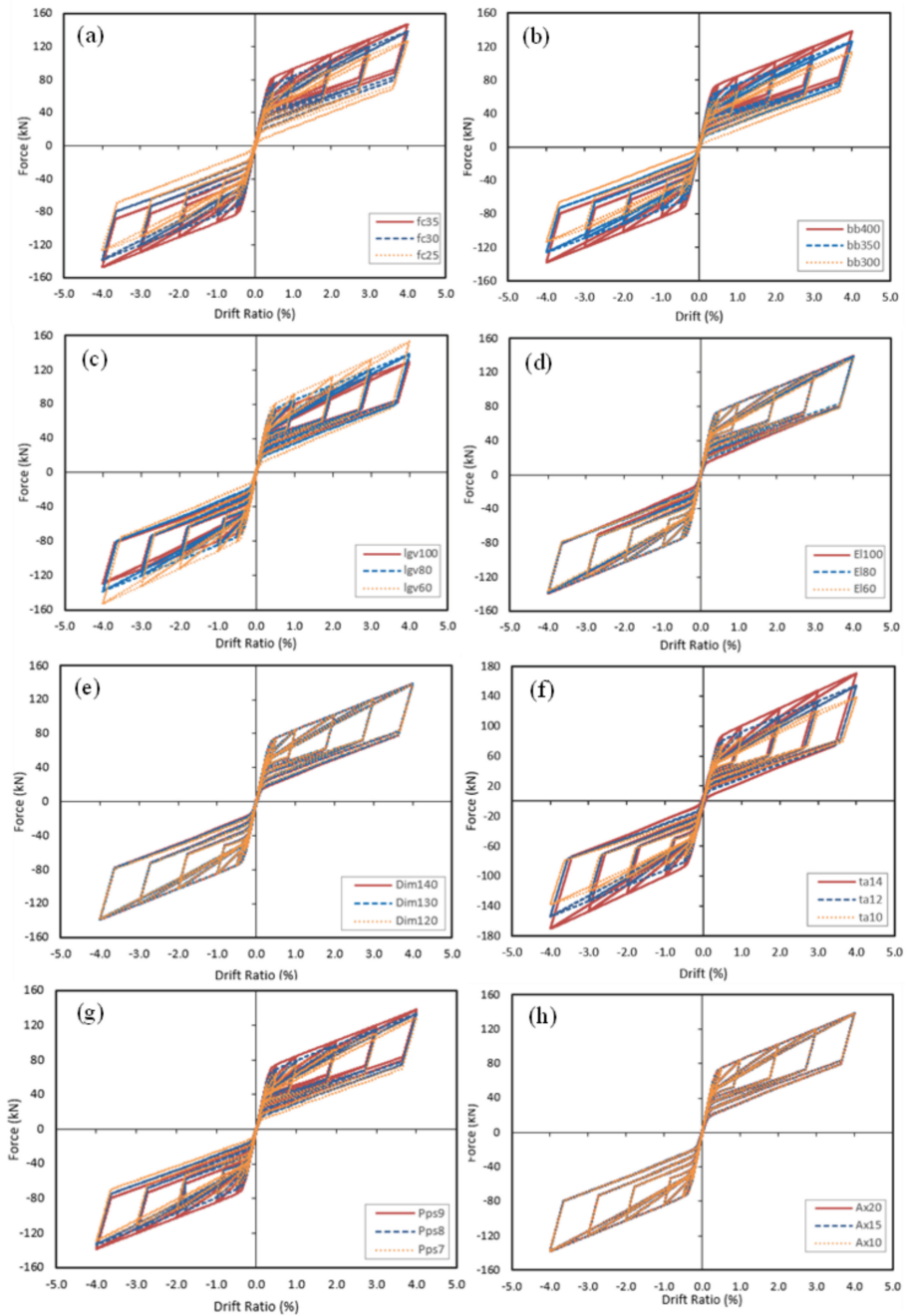


Fig. 7. Hysteresis curves result from the parametric study

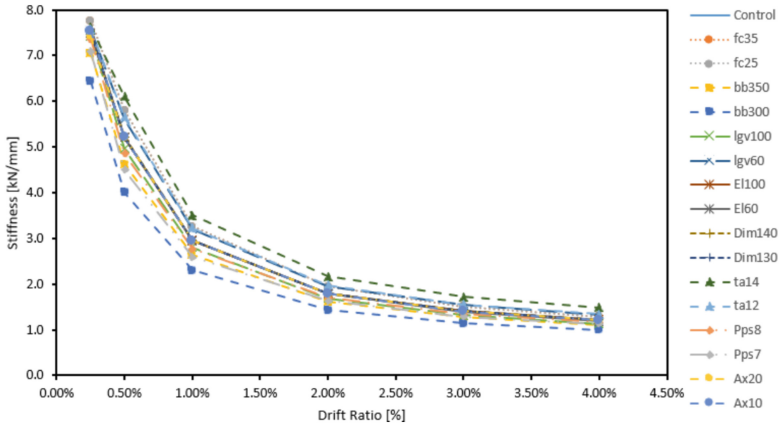


Fig. 8. Initial stiffness and stiffness degradation

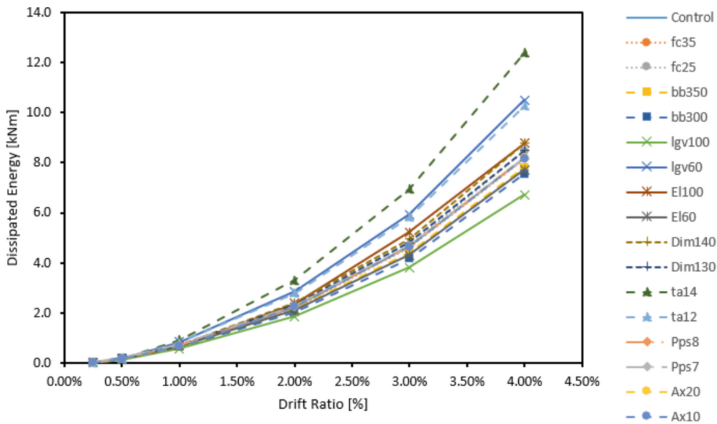
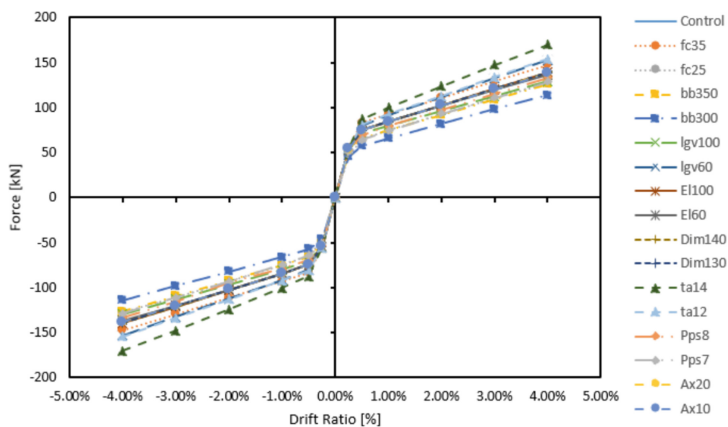


Fig. 9. Energy dissipation capacity

Table 6 shows complete results of the parametric study. As can be seen, steel angle thickness is the most influential parameter in the behavior of precast concrete interior beam-column joints with hybrid connection system. Increasing steel angle thickness from 10 mm to 14 mm can increase the maximum force by 22.97% and energy dissipation capacity by 51.18%. Besides steel angle thickness, concrete beam's width also has significant impact for the force capacity of the connection. Reducing beam's width ( $b_b$ ) from 400 mm to 300 mm, which also implies reducing steel angle width ( $b_a$ ), deduces the yielding force by 24.42% and maximum force by 17.81%. Moreover, for energy dissipation capacity, the distance of the first bolt at column leg also plays a significant role. Reducing the distance by 20 mm increases energy dissipation capacity by 28.04% whereas increasing the distance by 20 mm reduces energy dissipation capacity by 17.94%. These trends were also observed in the study by Cai et al. [16] for exterior beam-column joints.



**Fig. 10.** Backbone curves of all specimens

**Table 6.** Analysis results of the parametric study

Specimen	$P_{yield}$	Percentage Difference	$P_{max}$	Percentage Difference	Initial Stiffness	Percentage Difference	Energy Dissipation	Percentage Difference
	(kN)	(%)	(kN)	(%)	(kN/mm)	(%)	(kN.m)	(%)
Control	71.44	-	138.40	-	7.62	-	8.20	-
fc35	80.39	+12.53	147.35	+6.47	7.88	+3.44	8.16	-0.45
fc25	61.86	-13.41	127.09	-8.17	8.63	+13.25	8.47	+3.32
bb350	62.67	-12.28	126.42	-8.65	7.16	-6.07	7.79	-4.99
bb300	53.99	-24.42	113.75	-17.81	6.52	-14.44	7.55	-7.92
lgv100	67.95	-4.88	129.38	-6.51	6.87	-9.89	6.73	-17.94
lgv60	77.18	+8.04	152.95	+10.52	6.79	-10.90	10.50	+28.04
El100	71.42	-0.03	139.39	+0.72	7.63	+0.04	8.77	+6.97
El60	71.51	+0.10	136.28	-1.53	7.62	-0.04	7.72	-5.88
Dim140	71.51	+0.09	139.09	+0.50	7.64	+0.17	8.78	+7.10
Dim130	71.47	+0.05	138.75	+0.25	7.63	+0.08	8.49	+3.56
ta14	84.42	+18.17	170.19	+22.97	7.78	+2.10	12.40	+51.18
ta12	77.79	+8.88	154.23	+11.44	7.71	+1.19	10.27	+25.21
Pps8	65.98	-7.65	133.67	-3.42	7.47	-1.95	8.18	-0.26
Pps7	60.53	-15.27	128.89	-6.87	7.17	-5.91	8.18	-0.19
Ax20	71.49	+0.06	138.46	+0.04	7.54	-1.07	8.22	+0.21
Ax10	71.44	-0.01	138.25	-0.11	7.66	+0.44	8.17	-0.41

## 4 Conclusions

Numerical modeling and parametric study of precast concrete interior beam-column joints with hybrid connection system that combines unbonded post-tensioned strands and bolted steel angles were presented in this paper. From the results of this study, several concluding remarks can be summarized as follows:

- The numerical model of precast concrete interior beam-column joints with hybrid connection system was successfully developed. The model's validation shows that the numerical model is able to predict well the hysteresis behavior of the hybrid connection system under cyclic loading, including yielding and peak forces of the specimens. In addition, the numerical model successfully shows the self-centering characteristic with minimum residual drift and sufficient energy dissipation.
- Steel angle thickness was found to be the most influential parameter, profoundly impacting moment and energy dissipation capacities of the beam-column connections. Furthermore, concrete beam's width and the distance of the first bolt at column leg also have significant impact on force and energy dissipation capacities, respectively.

**Acknowledgements.** This study is a part of joint research project between Petra Christian University and P.T. Delta Utracon Synergy. The authors are grateful for the support and funding provided.

## References

1. American Society of Civil Engineers: ASCE standard ASCE/SEI 41-13 Seismic evaluation and retrofit of existing buildings. Am. Soc. Civil Eng. (2014). <https://doi.org/10.1061/9780784412855>
2. Federal Emergency Management Agency (FEMA): Seismic Performance Assessment of Buildings, vol. 1. Report No. FEMA P-58-1, Washington DC (2012)
3. Priestley, M.N., Tao, J.R.: Seismic response of precast prestressed concrete frames with partially debonded tendons. *PCI J.* **38**(1), 58–69 (1993). <https://doi.org/10.15554/pcij.01011993.58.69>
4. MacRae, G.A., Priestley, M.J.N.: Precast Post-Tensioned UngROUTED Concrete Beam-Column Subassembly Tests. Department of Applied Mechanics & Engineering Sciences, University of California, San Diego (1994)
5. Priestley, M.J.N., MacRae, G.A.: Seismic tests of precast beam-to-column joint sub-assemblages with unbonded tendons. *PCI J.* **41**(1), 64–81 (1996)
6. Stanton, J., Stone, W., Cheok, G.S.: A hybrid reinforced precast frame for seismic regions. *PCI J.* **42**, 20–32 (1993). <https://doi.org/10.15554/pcij.03011997.20.23>
7. Rodgers, G.W., et al.: Investigation of Rocking Connections Designed for Damage Avoidance with High Force-to-Volume Energy Dissipation. University of Canterbury, Christchurch (2008)
8. Do Tien, T.: Experimental study on a new precast unbonded post-tensioned beam-column joint system with shear bracket. *J. Struct. Constr. Eng. Trans. AIJ* **74**(641), 1249–1257 (2009). <https://doi.org/10.3130/aijs.74.1249>

9. Lachowicz, M., Nagrodzka-Godycka, K.: Experimental study of the post-tensioned prestressed concrete corbels. *Eng. Struct.* **108**, 1–11 (2016). <https://doi.org/10.1016/j.engstruct.2015.11.007>
10. Xu, X., Zhang, Y., Luo, Y.: Self-centering eccentrically braced frames using shape memory alloy bolts and post-tensioned tendons. *J. Constr. Steel Res.* **125**, 190–204 (2016). <https://doi.org/10.1016/j.jcsr.2016.06.017>
11. Chowdhury, M.A., Rahmzadeh, A., Moradi, S., Alam, M.S.: Feasibility of using reduced length superelastic shape memory alloy strands in post-tensioned steel beam-column connections. *J. Intell. Mater. Syst. Struct.* **30**(2), 283–307 (2019). <https://doi.org/10.1177/1045389X18806393>
12. Tazarv, M., Boudaqa, A., Tuhin, I.: Repairable precast moment-resisting buildings: part ii—analytical investigations. *ACI Struct. J.* **117**(6), 161–170 (2020). <https://doi.org/10.14359/51728062>
13. Huang, L., Zhou, Z., Clayton, P.M., Zeng, B., Qiu, J.: Experimental investigation of friction-damped self-centering prestressed concrete beam-column connections with hidden corbels. *J. Struct. Eng.* **146**(3), 04019228 (2020). [https://doi.org/10.1061/\(ASCE\)ST.1943-541X.0002536](https://doi.org/10.1061/(ASCE)ST.1943-541X.0002536)
14. Ricles, J.M., Sause, R., Garlock, M.M., Zhao, C.: Post-tensioned seismic-resistant connections for steel frames. *J. Struct. Eng.* **127**(2), 113–121 (2001). [https://doi.org/10.1061/\(ASCE\)0733-9445\(2001\)127:2\(113\)](https://doi.org/10.1061/(ASCE)0733-9445(2001)127:2(113))
15. Garlock, M.M., Sause, R., Ricles, J.M.: Behavior and design of post-tensioned steel frame systems. *J. Struct. Eng.* **133**(3), 389–399 (2007). [https://doi.org/10.1061/\(ASCE\)0733-9445\(2007\)133:3\(389\)](https://doi.org/10.1061/(ASCE)0733-9445(2007)133:3(389))
16. Cai, X., Gong, N., Fu, C.C., Zhu, Y., Wu, J.: Seismic behavior of self-centering prestressed precast concrete frame subassembly using steel top and seat angles. *Eng. Struct.* **229** (2021). <https://doi.org/10.1016/j.engstruct.2020.111646>
17. Wu, Z., Lu, X., Li, L., Bao, H., Lu, Z., Yu, K.: Seismic performance of full-scale self-centering reinforced concrete beam-column joints: experimental, numerical and theoretical analysis. *J. Build. Eng.* **78**, 107683 (2023). <https://doi.org/10.1016/j.jobe.2023.107683>
18. El-Sheikh, M., Pessiki, S., Sause, R., Lu, L.W.: Moment rotation behavior of unbonded post-tensioned precast concrete beam-column connections. *ACI Struct. J.* **97**(1), 122–131 (2000). <https://doi.org/10.14359/841>
19. Garlock, M.M., Ricles, J.M., Sause, R.: Cyclic load tests and analysis of bolted top-and-seat angle connections. *J. Struct. Eng.* **129**(12), 1615–1625 (2003). [https://doi.org/10.1061/\(ASCE\)0733-9445\(2003\)129:12\(1615\)](https://doi.org/10.1061/(ASCE)0733-9445(2003)129:12(1615))
20. Song, L.L., Guo, T., Chen, C.: Experimental and numerical study of a self-centering prestressed concrete moment resisting frame connection with bolted web friction devices. *Earthquake Eng. Struct. Dynam.* **43**(4), 529–545 (2014). <https://doi.org/10.1002/eqe.2358>
21. Lu, X., Cui, Y., Liu, J., Gao, W.: Shaking table test and numerical simulation of a 1/2-scale self-centering reinforced concrete frame. *Earthquake Eng. Struct. Dynam.* **44**(12), 1899–1917 (2015). <https://doi.org/10.1002/eqe.2560>
22. Cai, X., Pan, Z., Zhu, Y., Gong, N., Wang, Y.: Experimental and numerical investigations of self-centering post-tensioned precast beam-to-column connections with steel top and seat angles. *Eng. Struct.* **226** (2021). <https://doi.org/10.1016/j.engstruct.2020.111397>